Vine Vigour Characterization using a Multi-temporal X-band SAR Very High Resolution dataset

Guillaume Roussel, Lionel Bombrun, Christian Germain, Jean-Charles Samalens, Marc Spigai

Vine Vigour Characterization using a Multi-temporal X-band SAR Very High Resolution dataset

Guillaume Roussel[1], Lionel Bombrun[1], Christian Germain[1], Jean-Charles Samalens[2], Marc Spigai[3]

***Abstract*—In the vine-growing industry, the regular acquisition of image data throughout the vine-growing season is of great interest for accurate plot monitoring and grape yield prediction. In this context SAR backscattering data, which can be acquired at any time without being affected by clouds or night-time, seems particularly suitable, especially as their spatial resolution has significantly increased over the past few years. In this paper, we investigate the ability of X-band very high resolution (1 meter) SAR backscattering signal to characterize vine-plots. For that purpose, we used a multi-temporal dataset in order to study three vine-related factors : vine variety, ranks orientation and vine vigour. In our case, we want to monitor a known area for which vine variety and ranks orientation are well defined. As a consequence, we decided to focus on the most useful factor for vine-growers, i.e. vine vigour. The methodology used is a whole sensitivity analysis over a vine vigour classification and regularization process by using only the amplitude of the SAR backscattering.**

I. Introduction

In agricultural and forestry sciences, remote sensing is a major asset for the monitoring and global management of wide plots. It is involved in many applications, from land occupation to the inspection of declared areas, the evaluation of productivity - estimating various agronomic factors such as vigour and ground type - or the study of the impact of climatic events, such as drought, flood and frost, on crops.

For vineyard monitoring in particular, optical remote sensing has been widely used. Delenne et al. [7] and Rabatel et al. [18] have computed a very efficient method to detect, delineate and characterize vine plots using Fast Fourier Transform (FFT). Homayouni et al. [13] use a spatial/spectral method to compute vegetation abundance maps, which comes down to abundance-weighted vigour indexes allowing accurate vigour mapping. Chanussot et al. [6] exploit the periodic structure of vineyard to identify dead or missing trees using FFT, Radon Transform and morphological operators. Some classification applications also exist. Senturk et al. [21] use a hierarchical clustering approach based on self-organizing neural networks, in which they integrate both spectral and textural (Gabor features) bands to distinguish vine plots from other crop classes. On the other hand, Lacar et al. [15] proposed a Maximum Likelihood approach to discriminate two vine varieties (Cabernet Sauvignon and Shiraz). Finally, a few studies have been conducted on the characterization of vineyard factors such as Leaf Area Index (LAI) or canopy shape [12], [24].

However, when the weather is cloudy or during night-time, multispectral or hyperspectral space-borne data cannot be acquired. This can be a problem when regular data acquisition are required, for instance in a vine-growing context. In this particular situation, the interest of Synthetic Aperture Radar (SAR) sensors grows significantly since their waves propagate through cloud layers with a very small attenuation. Despite that, their potential is not used in daily-based operational processing in the agricultural field, mainly because of both the complexity of SAR image interpretation (regarding speckle and acquisition geometry) and the low spatial resolution making difficult the observation of small objects such as vine. A few studies try to highlight the relation between the LAI of cereal plots and polarimetric parameters [8], [11]. As for Shang et al. [22], they analyzed the complementarity between SAR and optical data, coming up with the fact that SAR signal informs on crop structures (size, shape, orientation) and to canopy dielectric properties, whereas optical signal answer to plant biochemical structure and biomass level. Thanks to the most recent very high resolution (VHR) SAR sensors, the texture information become visible (at least for several applications) and treatable. For forestry applications, Champion et al. [5] managed to find a good correlation between several Haralick's features (energy and entropy) and forest plot stand age classes.

For vineyard monitoring, publications taking advantage of SAR imagery are even rarer. In [20], Schiavon et al. have addressed the potential of L-band and C-band SAR backscattering for the classification of harvested areas using E-SAR data (2m resolution). Their results are hinting at a sensitivity of L-band backscattering to grape biomass per unit area but they add that a number of disturbing effects were detrimental to their accuracy. Burini et al. [4] combine optical and SAR L-band data to retrieve biophysical factors such as LAI but they explicitly say that LAI is uncorrelated to the radar backscattering signal alone at these frequencies. In [1], Baghdadi et al. use that L- and P-band SAR data acquired in winter, which proved to be not suitable to characterize vine age and rank direction. All these studies focus on low frequency radar sensors (P, L and C) with medium resolutions. Del Frate et al. [10] use SAR X-band VHR data to successfully characterize vine vigour but SAR data is processed together with optical data, which can be impossible to get by night or if the weather is cloudy.

Nowaday, the most performant SAR sensors such as Cosmo-Skymed or TerraSAR-X allow a spatial resolution of 1 meter. The purpose of this study is to evaluate the

[1] Laboratoire IMS, Université de Bordeaux
[2] Telespazio France, Latresne
[3] Thales Alena Space, Toulouse

Figure 1. Working Area

potential of X-band VHR SAR imagery for plot and intra-plot vineyard characterization by studying the relation between vine vigour and SAR signal backscattering amplitude along with its evolution over time according to vine phenological states. First, the ground data and images datasets are described. Then each factor is evaluated individually over the whole studied area and finally, section 4 is dedicated to the analysis of the vineyard vigour while the other factors are fixed.

II. Datasets and preliminary works

The studied area is located approximately thirty kilometers east of Agen, in France (cf. figure 1). It is composed of thirty-six vineyard plots with various orientations and vine varieties, and a relatively high average slope intensity ($\approx 10°$).

A. Cosmo-Skymed images and pre-processing

For this study, we had access to optical and SAR images, along with various ground data, all provided by Telespazio (EarthLab project). Our main dataset is composed of fourteen X-band Cosmo-Skymed images. In order to evaluate the temporal evolution of SAR signal backscattering, these images have been registered on a rolling basis on a period covering the beginning of May 2013 (leaves appearance) to the end of September 2013 (harvesting). Each image have been acquired with SPOTLIGHT mode, which implies a ground coverage of 10km × 10km, a spatial resolution slightly lower than one meter and HH polarization. In theory, cross-polarization (HV) is a better choice for vegetation monitoring [2], but choosing such a polarization would have forced us to work with lower resolution data (very high resolution Cosmo-Skymed data exist only with HH or VV polarization), which wasn't optimal regarding the size of the plots we are working on. The incidence angle varies between 22° for the closest pixels (regarding the sensor) to 23° for the most distant ones. In the COSMO SAR nomenclature, these images correspond to level 1A standard products, i.e. complex data which haven't been georeferenced yet. Georeferencing is done using the NEST software provided by the European Space Agency (ESA). The process use a portion (corresponding to the ground coverage of the images) of the global digital elevation model (DEM) SRTM3 to reproject the data according to the geodetic datum WGS84 and the projection UTM31. It also performs a radiometric calibration (σ_0) and a speckle filtering, using a Lee filter [16]. Finally, a radiometric correction regarding the local slope of each pixel is used, through Matlab. Indeed, the local slope in the range direction affects the surface area covered by a pixel, which affects the signal value registered by the sensor. To reduce this effect, the method proposed by Luckman et al. [17] is applied :

$$C(\sigma_0) = \sigma_0 \sin(\Theta_{DEM}) \tag{1}$$

where σ_0 is the orthorectified sigma nought, $C(\sigma_0)$ the corrected sigma nought and Θ_{DEM} the local incident angle associated to each pixel.

B. Vineyard factors characterization

The study focus on three vineyard factors : vine variety, rank orientation and vine vigour. Since every vines in the same vineyard belong to the same vine variety, this latter can be considered as a plot-wise factor. Ground data consists in a cadastral database (cf. figure 2a) characterizing each plot by one variety among three : Cabernet Sauvignon, Cabernet Franc and Merlot. Vine vigour is a pixel-wise factor consisting in a NDVI map of the area classified in order to highlight three different levels of vigour (cf. figure 2b). This NDVI map have been processed from a Geo-Eye multispectral image with a spatial resolution of half a meter, acquired at the beginning of July. The ground data for the rank orientation factor (plot-wise) was created using the same Geo-Eye image, on which a semi-automatic method based on Gabor filter banks [14] was applied. This method consists in applying a set of Gabor filters with different orientations (from 0° to 179°) to the image and then to choose for each plot the orientation which resulted in the highest contrast.

For each factor, each class and each date, the mean and the standard deviation of $C(\sigma_0)$ were computed in order to study its evolution over time, from the beginning to the end of the season (cf. figure 3). On these charts, most of the classes show different mean $C(\sigma_0)$ values. However, the standard deviation of the distributions are too wide and overlap too much to make the discrimination between the classes possible, at least for a pixel-wise process. The main issue of this method lies in the potential interdependencies existing between the vineyard factors. For example, a mean curve associated to a single vine vigour class is created from a set of pixels with different rank orientations and vine varieties, which can prevent a proper evaluation of the influence of the vine vigour factor on the SAR backscattering signal.

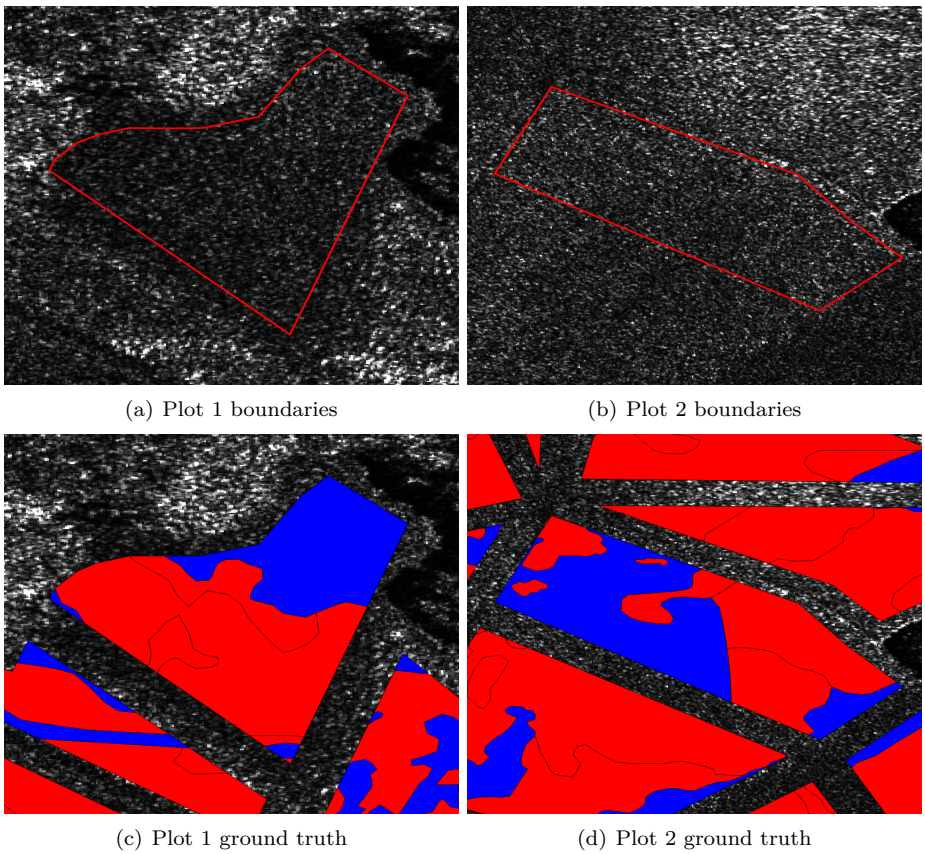

(a) Plot 1 boundaries (b) Plot 2 boundaries

(c) Plot 1 ground truth (d) Plot 2 ground truth

Figure 4. Working plots, with high vigour areas in blue and low vigour areas in red

III. Vine vigour classification : a sensitivity analysis

Starting from the hypothesis that the vineyard factors studied in this paper were potentially correlated, we decided to simplify the problem by studying a single factor while fixing the two others. Among the three factors mentioned in the previous section, we focus on the vine vigour, considering that it is the most interesting one for wine-growers.

A. Methodology

The following sensitivity analysis aims to evaluate the ability of VHR X-band SAR images to quantify vine vigour when rank orientation and vine variety (plot-wise and easier to get as ground data) are fixed. To do so, the plots are processed one by one instead of considering the whole image at once. Two plots are considered in the study (c.f. figure 4). They have been chosen over all other plots because they present a good variability in terms of vine vigour. The two plots differ in their vine variety and the intensity of their slope. Plot 1 is relatively flat and plot 2 is twice as steep.

Considering their strong similarity on figure 3b, the medium and low vigour classes have been fused in one class. Since the vigour ground data has been computed from a Geo-Eye image acquired at the beginning of July, the proposed methodology is applied on a single SAR dataset acquired the seventh of July 2013.

Finally, two pre-processing have been applied (or not) to the data : Speckle filtering and orthorectification. In the first case, we tested several sizes of Lee filters (from 7×7 to 19×19) and in the second case, the classification process is launched either on slant data or on orthorectified data.

1) Classification algorithms: The classification algorithms described in this paper are all supervised, meaning that a prior knowledge is used to build a model which will be able to infer the class of every pixel in the image. This prior knowledge consist in a set of learning samples, i.e. pixels whose class is known from the ground data. In order to reflect realistically the acquisition conditions of the ground data, learning samples have been chosen as connex and localized set of pixels. Two algorithms have been compared.

The first one is the SVM (*Support Vector Machine*) algorithm [3], a widely used tool which present the interest of being efficient even if the learning samples set is small. For an image classification problem, this algorithm aims to compute an hyperplane or a set of hyperplanes in the dimensional space formed by the image bands, which best separate a finite number of classes. It is able to address non linearly separable cases using a kernel function (in our case, we use the RBF kernel) which map the original data space into a higher dimensional space where the separation is easier. However, this method is optimised for gaussian distributions whereas SAR intensity images are more commonly associated with Gamma distributions.

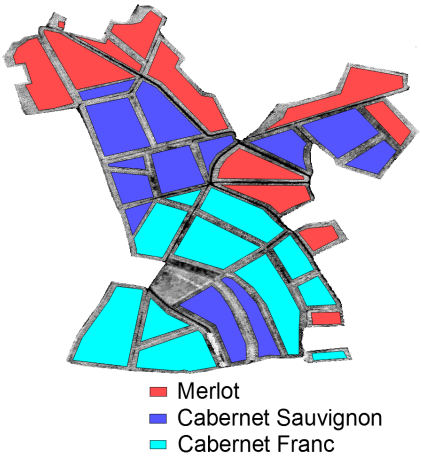

(a) Vine variety ground truth

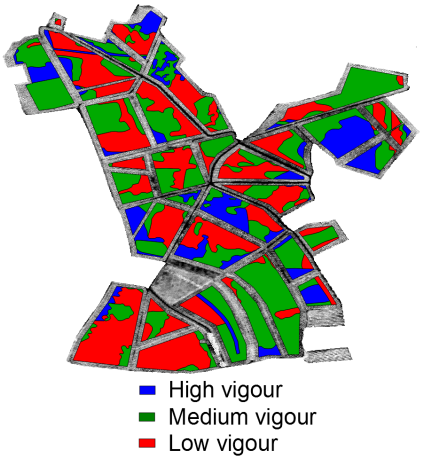

(b) Vine vigour ground truth

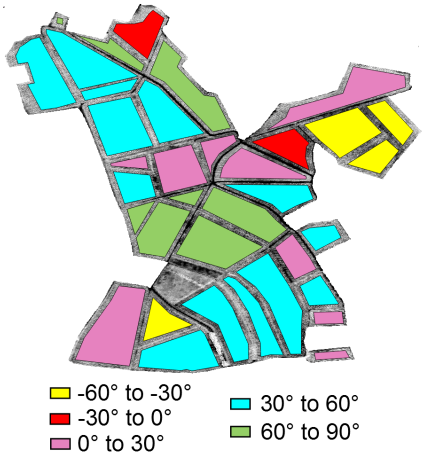

(c) Rank orientation ground truth

Figure 2. Ground truth maps

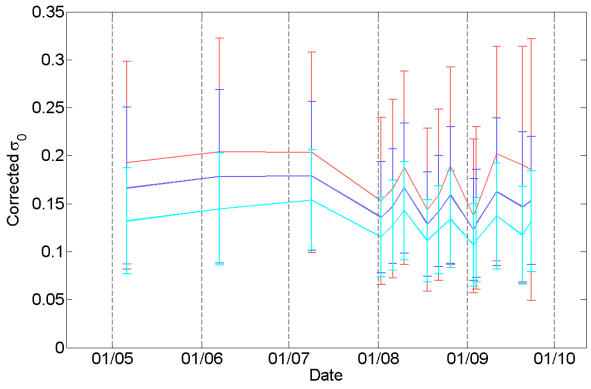

(a) Vine variety : Merlot (red), Cabernet Sauvignon (purple), Cabernet Franc (cyan)

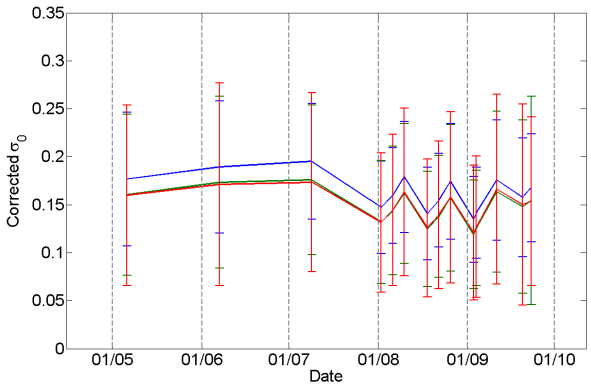

(b) Vine vigour : High (blue), Medium (green), Low (red)

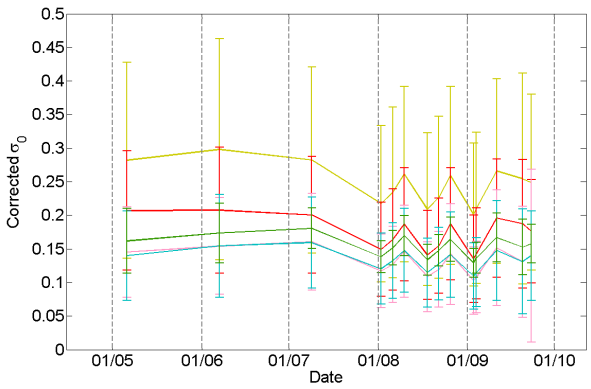

(c) Rank orientation : −60° to −30° (yellow), −30° to 0° (red), 0° to 30° (pink), 30° to 60° (cyan), 60° to 90° (green)

Figure 3. Evolution of the mean $C(\sigma_0)$ value (with the associated standard deviation) through time. Each curve represent a specific class of the vineyard factor associated to the chart.

Consequently, a second classification method have been included in the study, a maximum likelihood algorithm associated with a Gamma law. The first step of this algorithm consists in estimating for each class c the parameters k_c and θ_c of a Gamma distribution using the learning samples set (learning phase). Here is the probability density function of the Gamma distribution :

$$f_\Gamma(x;k,\theta) = \frac{x^{k-1}e^{-\frac{x}{\theta}}}{\theta^k \Gamma(k)} \tag{2}$$

Then the label of each pixel is inferred by using the maximum likelihood principle :

$$\hat{c} = \text{argmax}_c \log f_\Gamma(x_p; k, \theta) \quad (3)$$

where p is a pixel, x_p its value in the image and $\Gamma(\cdot)$ is the Gamma function.

2) Rejection class: Even after the fusion of two vigour classes, we remarked that the distributions associated to the two remaining classes were very similar to each other. In [9], Formont et al. add a rejection class in the classification process in order to put aside the pixels for which the label is uncertain and improve the classification results. Such a method can be adapted to the maximum likelihood algorithm. The uncertainty thresholds are computed as follows (cf. figure 5). If X_1 and X_2 are two gamma-distributed random variables associated respectively to classes c_1 and c_2, with $E(X_1) < E(X_2)$, the objective is to determine the abscissa t_1 and t_2 such as $\alpha_1 = P(X_1 > t_1)$ and $\alpha_2 = P(X_2 < t_2)$, with $\alpha_1, \alpha_2 \in]0, 1[$ and $\alpha_1 = \alpha_2$. t_1 and t_2 are then directly estimated from the inverse cumulative distribution function of the Gamma law. Finally for p a pixel of the image, we got three possibilities :

- $p < t_2 \Longrightarrow p \in c_1$
- $p > t_1 \Longrightarrow p \in c_2$
- $t_2 < p < t_1 \Longrightarrow p \in c_r$, where c_r is the rejection class

Several values have been tested for α_1 and α_2 : 0.025, 0.05 and 0.1.

3) Regularization algorithms: Then, three regularization methods have been tested. The first one (MR) is based on the mathematical morphology theory and consist in applying successively two morphologic operators on the classification result : an opening and a closing by reconstruction [19]. Unlike classical opening and closing operators, these reconstruction operators do not deform excessively the objects in the image : either the object is deleted if it is too small, or it is completely preserved. The second approach is a majority voting [23] algorithm (MV) : each pixel is labelled with the most commonly represented class in its neighbourhood. Both methods work with a sliding window which scans every pixel in the image and for which several sizes have been tested (3, 7 and 11). Finally, the last method is a markovian approach working on the basis of a simulated annealing. This method requires the parameters k and θ computed in section III-A1 and is based on the ICM (Iterative Conditional Modes) algorithm which aims to minimize an energy composed of a data term and a regularization term. This energy is processed for each pixel p and each label c :

$$E(p, c) = -\log f_\Gamma(x_p; k, \theta) + \sum_{v \in V_p} N(v, c) \quad (4)$$

$$N(v, c) = \begin{cases} \beta, c \neq y_v \\ -\beta, c = y_v \end{cases} \quad (5)$$

where V_p is a set including the eight neighbours of p and y_v is the label associated with pixel v in the classification map Y. The first term in (4) is a data fidelity term while the second one is a regularization term which penalizes non smooth regions. Then, y_p is updated with the label c which minimize $E(p, c)$ and the whole process is repeated until convergence (no more change).

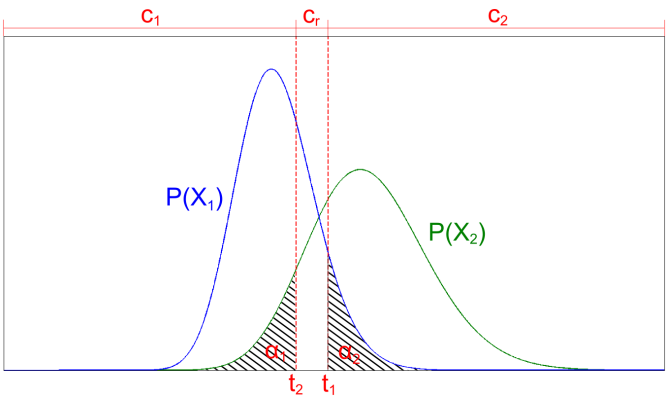

Figure 5. Threshold selection for rejection class definition

B. Results

Table I presents the results obtained on univariate data, without any rejection class. Concerning plot 1, we can notice that the classification accuracy grows with the size of the sliding windows used for speckle filtering and regularization, but hardly exceed 70%, while for plot 2 the accuracy is very low and usually not improved by the regularization step. The results obtained by the two classification algorithms are rather similar, with a subtle advantage for MLE. Note that more general univariate models may be considered such as Fisher. However, for this particular application, this law haven't lead to significant gain regarding the classification performances. In terms of regularization, it's the majority voting algorithm which distinguish itself. ICM only leads to superficial improvements while the morphological reconstruction algorithm is likely to erase completely some areas when the sliding window is too large. Finally, regularized classification maps are more accurate when they are built from slant data, even if the improvement is again very subtle.

Table II show the results obtained when a rejection class is included to the problem. The integration of such a class can eventually lead to a situation where test samples sets do not include the same number of elements. In table I, the accuracy measure used is the overall accuracy, which calculate the global percentage of well-classified pixels. This measure is relevant when the number of test samples is equivalent for each class but can be misleading otherwise. The average accuracy, which process the percentages on each class before averaging them, is a much more pertinent choice in this case.

Several conclusions can be drawn from table II. First, the proportion of rejected pixels is each time approximately 15% higher for orthorectified data than for slant data, which seems to confirm that the orthorectification process reduces the differences between classes. On plot

2, this proportion is consistently large without leading to an accuracy improvement, while for plot 1, the rejection proportion is more acceptable when α_1 and α_2 are high enough. However, the accuracy is then nearly the same than without rejection class.

IV. Conclusion and discussion

In this paper, we aimed to evaluate the potential of X-band SAR VHR imagery to characterize vine vigour by using multi-temporal data and amplitude as input of the processing. At first we studied vine variety, ranks orientation and vine vigour individually, comparing the evolution of their classes from the beginning to the end of a wine-making season. However, even though each of them seems to have an incidence over SAR signal backscattering, the disparity between their classes is not large enough to discriminate them. Assuming the existence of inter-dependencies between those three factors, we then focus on a single factor (vine vigour) while fixing the others. A whole sensitivity analysis have been conducted on the wine vigour classification to determine the ability of VHR X-band SAR imagery to characterize this factor. Several axis have been taken into account in the analysis : classification algorithm, regularization algorithm, geometry, speckle filtering and rejection threshold. At the end for this particular application, the maximum likelihood method showed slightly better results than the SVM classifier and the most efficient regularization algorithm is the majority voting. Furthermore, the slant geometry appears to be better to discriminate the different classes of vigour. However, on the studied area and with the data available, the relationship between X-band SAR signal amplitude and vine vigour doesn't seem to be significant enough to build a prediction model. This assessment should nevertheless be taken with care. Indeed the weak incidence angle of our data may give too much influence to the ground in the backscattering process. A steeper angle may help to focus more on the vine canopy. On the other hand, using cross-polarized data - known to be the best choice for plant targets, but unfortunately unavailable with VHR Cosmo-Skymed images - instead of co-polarized data may also result in a more precise characterization of the vine, which would help increasing the accuracy of the vine vigour classification process. Finally, acquisitions in interferometric conditions, which is possible in a 4days-15days revisit time basis with Cosmo-Skymed constellation, would allow to compute a coherence map all along the serie acquisition. The lost or gain of coherence between each coherence map may eventually bring useful information to characterize the vigour.

Acknowledgements

The authors would like to thank Telespazio EarthLab Project for the financial support and for authorizing the use of both image (Cosmo-Skymed and Geo-Eye) and ground data (vine variety and vigour).

References

[1] N. Baghdadi, N. Holah, P. Dubois-Fernandez, X. Dupuis, and F. Garestier. Evaluation of polarimetric l- and p-band ramses data for characterizing mediterranean vineyards. In *Can. J. Remote Sensing*, volume 32, pages 380–389, 2006.

[2] J.D. Ballester-Berman, J.M. Lopez-Sanchez, I Garmendia-Lopez, and V.J. Mangas-Martin. Incoherent electromagnetic model for vineyards at c-band. In *Geoscience and Remote Sensing Symposium (IGARSS), 2012 IEEE International*, pages 5689–5692, July 2012.

[3] ChristopherJ.C. Burges. A tutorial on support vector machines for pattern recognition. *Data Mining and Knowledge Discovery*, 2(2):121–167, 1998.

[4] A Burini, G. Schiavon, and D. Solimini. Fusion of high resolution polarimetric sar and multi-spectral optical data for precision viticulure. In *Geoscience and Remote Sensing Symposium, 2008. IGARSS 2008. IEEE International*, volume 3, pages III – 1000–III – 1003, July 2008.

[5] I Champion, C. Germain, J.P. Da Costa, A Alborini, and P. Dubois-Fernandez. Retrieval of forest stand age from sar image texture for varying distance and orientation values of the gray level co-occurrence matrix. *Geoscience and Remote Sensing Letters, IEEE*, 11(1):5–9, Jan 2014.

[6] Jocelyn Chanussot, Patrick Bas, and Lionel Bombrun. Airborne remote sensing of vineyards for the detection of dead vine trees. In *IGARSS*, pages 3090–3093. IEEE, 2005.

[7] Carole Delenne, Sylvie Durrieu, Gilles Rabatel, and Michel Deshayes. From pixel to vine parcel: A complete methodology for vineyard delineation and characterization using remote-sensing data. *Computers and Electronics in Agriculture*, 70(1):78 – 83, 2010.

[8] Laura Dente, Giuseppe Satalino, Francesco Mattia, and Michele Rinaldi. Assimilation of leaf area index derived from {ASAR} and {MERIS} data into ceres-wheat model to map wheat yield. *Remote Sensing of Environment*, 112(4):1395 – 1407, 2008. Remote Sensing Data Assimilation Special Issue.

[9] P. Formont, F. Pascal, G. Vasile, J. Ovarlez, and L. Ferro-Famil. Statistical classification for heterogeneous polarimetric sar images. *Selected Topics in Signal Processing, IEEE Journal of*, 5(3):567–576, June 2011.

[10] Fabio Del Frate, Daniele Latini, Matteo Picchiani, Giovanni Schiavon, and Cristina Vittucci. A neural network architecture combining vhr sar and multispectral data for precision farming in viticulture. 2014.

[11] R. Hadria, B. Duchemin, L. Jarlan, G. Dedieu, F. Baup, S. Khabba, A. Olioso, and T. Le Toan. Potentiality of optical and radar satellite data at high spatio-temporal resolutions for the monitoring of irrigated wheat crops in morocco. *International Journal of Applied Earth Observation and Geoinformation*, 12, Supplement 1(0):S32 – S37, 2010. Supplement Issue on.

[12] Andrew Hall, John Louis, and David Lamb. Characterising and mapping vineyard canopy using high-spatial-resolution aerial multispectral images. *Computers and Geosciences*, 29(7):813 – 822, 2003.

[13] Saeid Homayouni, Christian Germain, Olivier Lavialle, Gilbert Grenier, Jean-Pascal Goutouly, Cornelis Van Leeuwen, and Jean-Pierre Da Costa. Abundance weighting for improved vegetation mapping in row crops: application to vineyard vigour monitoring. *Canadian Journal of Remote Sensing*, 34(S2):228–239, 2008.

[14] AK. Jain and F. Farrokhnia. Unsupervised texture segmentation using gabor filters. In *Systems, Man and Cybernetics, 1990. Conference Proceedings., IEEE International Conference on*, pages 14–19, Nov 1990.

[15] F. M. Lacar, M.M. Lewis, and I. T. Grierson. Use of hyperspectral imagery for mapping grape varieties in the barossa valley, south australia. In *Geoscience and Remote Sensing Symposium, 2001. IGARSS '01. IEEE 2001 International*, volume 6, pages 2875–2877 vol.6, 2001.

[16] Jong-Sen Lee. Digital image enhancement and noise filtering by use of local statistics. *Pattern Analysis and Machine Intelligence, IEEE Transactions on*, PAMI-2(2):165–168, March 1980.

Table I
RESULTS OBTAINED (OVERALL ACCURACY IN %) ON THE TWO PLOTS FOR VIGOUR CLASSIFICATION, WITH SLANT AND ORTHORECTIFIED DATA, SEVERAL CLASSIFICATION AND REGULARIZATION ALGORITHMS, AND SEVERAL LEE FILTER SIZES.

		Orthorectified data				Slant data			
		Plot 1		Plot 2		Plot 1		Plot 2	
Lee filter size		7×7	19×19	7×7	19×19	7×7	19×19	7×7	19×19
SVM	-	62.6	68.3	49.2	45.8	60.3	66.8	53.6	54.7
	MR3	64.6	68.8	49.7	45.6	64.4	70.7	56.4	66
	MR11	70.8	69	38.7	46.3	48.6	71.2	51.4	51.4
	MV3	65.5	69.1	48.6	45.4	65.4	69.7	55.1	57.5
	MV11	70.7	70.7	49.8	45.3	72.1	73.6	56	60
MLE	-	61.6	69	53.8	49.3	60.4	68.6	51.7	51.4
	ICM	63.2	69.3	54.6	49.3	62.2	69.1	52	52
	MR3	61.7	69.1	55.1	49.3	62.2	69	52.7	52.5
	MR11	70.1	69.9	38.7	49.6	48.6	72.4	51.4	51.7
	MV3	64	69.5	55.3	49.4	63.4	72.8	52.7	52.5
	MV11	70.7	71.3	57.8	49.6	71.1	74.9	51.2	51.4

Table II
RESULTS OBTAINED (IN %) ON THE TWO PLOTS FOR MLE VIGOUR CLASSIFICATION, WITH SLANT AND ORTHORECTIFIED DATA, SEVERAL REGULARIZATION ALGORITHMS (RA) AND INCLUDING A REJECTION CLASS ASSOCIATED WITH SEVERAL REJECTION THRESHOLDS (RT). DATA HAVE BEEN PREVIOUSLY FILTERED BY A 19×19 LEE FILTER. IN EACH CELL, THE FIRST NUMBER STANDS FOR THE AVERAGE ACCURACY AND THE NUMBER BETWEEN BRACKETS FOR THE REJECTION PROPORTION.

			Orthorectified data		Slant data	
CA	RT	RA	Plot 1	Plot 2	Plot 1	Plot 2
MLE	0.025%	-	73.4 (71.5)	43.2 (81.6)	68.5 (52.2)	55.8 (64.8)
		MV3	73.3 (72.8)	42.4 (83)	69.1 (53.9)	55.9 (66)
		MV11	77.7 (77.3)	40 (88.8)	74.2 (58.1)	55.9 (71.8)
	0.05%	-	72.6 (53.4)	46 (72.8)	68.2 (36.6)	56.2 (56.5)
		MV3	74.3 (54.7)	46.6 (74.8)	69.3 (37.6)	56.4 (58)
		MV11	79.7 (58)	43.6 (81)	73.7 (38.9)	56.4 (62.7)
	0.1%	-	69.5 (24.5)	47.6 (58.6)	67 (13.2)	56.5 (44.8)
		MV3	69.6 (24)	48.2 (59.5)	66.7 (9.1)	57 (46.2)
		MV11	72.2 (17.9)	48 (64.3)	69.7 (1.7)	58.8 (49.8)

[17] AJ. Luckman. Correction of sar imagery for variation in pixel scattering area caused by topography. *Geoscience and Remote Sensing, IEEE Transactions on*, 36(1):344–350, Jan 1998.

[18] Gilles Rabatel, Carole Delenne, and Michel Deshayes. A non-supervised approach using gabor filters for vine-plot detection in aerial images. *Computers and Electronics in Agriculture*, 62(2):159 – 168, 2008.

[19] P. Salembier and M. Pardas. Hierarchical morphological segmentation for image sequence coding. *Image Processing, IEEE Transactions on*, 3(5):639–651, Sep 1994.

[20] G. Schiavon, D. Solimini, and A. Burini. Sensitivity of multi-temporal high resolution polarimetric c and l-band sar to grapes in vineyards. In *Geoscience and Remote Sensing Symposium, 2007. IGARSS 2007. IEEE International*, pages 3651–3654, July 2007.

[21] S. Senturk, K. Tasdemir, S. Kaya, and E. Sertel. Unsupervised classification of vineyard parcels using spot5 images by utilizing spectral and textural features. In *Agro-Geoinformatics (Agro-Geoinformatics), 2013 Second International Conference on*, pages 61–65, Aug 2013.

[22] Jiali Shang, H. McNairn, C. Champagne, and Xianfeng Jiao. Contribution of multi-frequency, multi-sensor, and multi-temporal radar data to operational annual crop mapping. In *Geoscience and Remote Sensing Symposium, 2008. IGARSS 2008. IEEE International*, volume 3, pages III – 378–III – 381, July 2008.

[23] Y. Tarabalka, J. Chanussot, J.A Benediktsson, J. Angulo, and M. Fauvel. Segmentation and classification of hyperspectral data using watershed. In *Geoscience and Remote Sensing Symposium, 2008. IGARSS 2008. IEEE International*, volume 3, pages III – 652–III – 655, July 2008.

[24] P.J. Zarco-Tejada, A. Berjón, R. López-Lozano, J.R. Miller, P. Martín, V. Cachorro, M.R. González, and A. de Frutos. Assessing vineyard condition with hyperspectral indices: Leaf and canopy reflectance simulation in a row-structured discontinuous canopy. *Remote Sensing of Environment*, 99(3):271 – 287, 2005.